

On-site enhancement and control of spin-forbidden dark excitons in a plasmonic heterostructure

Received: 25 September 2024

Accepted: 26 September 2025

Published online: 12 November 2025

 Check for updates

Jiamin Quan^{1,6}, Michele Cotrufo¹, Saroj Chand¹, Xuefeng Jiang¹, Zhida Liu², Enrique Mejia¹, Wei Wang¹, Takashi Taniguchi³, Kenji Watanabe⁴, Gabriele Grosso^{1,5}, Xiaoqin Li²✉ & Andrea Alù^{1,5}✉

Dark excitons in atomically thin van der Waals materials provide an exciting platform for information transport and nanophotonic applications. Although dark excitons are difficult to access through free-space radiation, hybrid heterostructures incorporating plasmonic nanocavities provide a powerful platform to tailor their interactions with photons. Here we design a heterostructure consisting of optimized plasmonic nanocubes coupled to a WSe₂ monolayer encapsulated between thin hexagonal boron nitride layers to unveil a new family of dark excitons. The emission from these dark excitons is 2,700 times stronger than bright excitons, yielding a striking enhancement factor of 3×10^5 . We demonstrate the spin-forbidden nature of these dark states by studying their magneto-optical response. Furthermore, we selectively activate them by controlling the Fermi level via electric doping. Prominent features of these dark excitons include narrow linewidths, long lifetime, efficient electrical and magnetic modulation. Our findings unlock the potential for exploring exciton physics in two-dimensional materials using photonic heterostructures that preserve the intrinsic optical properties of two-dimensional materials in the coupling process. The demonstrated on-site control and ease of integration with passive photonic components make this platform particularly compelling for nanophotonic and sensing applications.

In monolayers of transition metal dichalcogenides (TMDs), the strong Coulomb interaction arising from weak dielectric screening and extreme quantum confinement results in prominent exciton states¹. Excitons can be either optically bright or dark, depending on the spin and momentum configuration of the electron–hole pairs². Spin-forbidden dark excitons, characterized by an out-of-plane dipole moment, undergo an additional spin-flip process to emit a photon, exhibiting significantly longer lifetimes, typically a few hundred picoseconds or longer. This feature makes them suitable for processing and transport applications^{3,4}. Plasmonic cavities, known for supporting strong out-of-plane field enhancements, have been reported to

enhance exciton emission in two-dimensional (2D) materials even at room temperature^{5–9}.

Dark exciton enhancement by plasmonic cavities, however, remains a subject of long-standing debate. First, plasmonic doping at the metal–TMD interface induces charge transfer^{10–15}. Various measurements, including near-field gap control¹⁶, lifetime measurement¹⁷, back-gated transfer characteristics¹⁵ and pump–probe experiments¹⁰, have led to the attribution of enhanced peaks observed in the plasmonic cavity–TMD hybridized structure to charge-transfer-induced trions, rather than to cavity-enhanced dark excitons. Second, dark excitons, with their intrinsically long lifetime, should exhibit a much

A full list of affiliations appears at the end of the paper. ✉ e-mail: elaineli@physics.utexas.edu; aalu@gc.cuny.edu

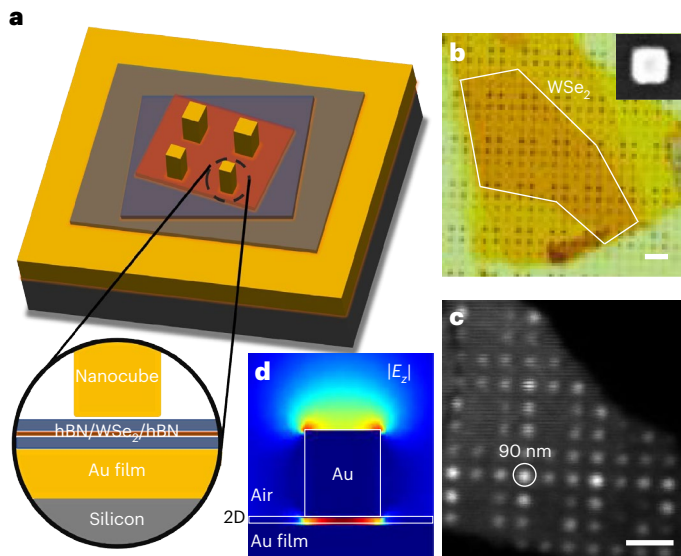


Fig. 1 | Plasmonic heterostructure and characterization. **a**, Schematic of the plasmonic nanocavity. The hBN-encapsulated WSe₂ monolayer is embedded between a nanocube and a flat Au layer. **b**, Optical microscopy image of an as-prepared sample. The white line encircles the monolayer WSe₂. Inset: scanning electron microscopy image of a nanocube with lateral size of 120 nm. **c**, PL mapping of a region containing antennas of different sizes. The signal is the sum of emissions from all exciton states. Scale bars, 2 μm (**b** and **c**). **d**, Calculated electric field of the eigenmode supported by a device with dimensions $90 \times 90 \times 100 \text{ nm}^3$. The total thickness of two hBN layers is 8 nm. The plot shows the magnitude of the vertical field component, $|E_z|$, in a vertical plane located in the middle of the nanocube. The magnitudes of the other field components are shown in Supplementary Fig. 1.

narrower linewidth compared with bright excitons^{18,19}. However, the reported enhanced dark exciton emission, when coupled to plasmonic structures, consistently exhibit a broad linewidth, resembling or even exceeding that of bright excitons^{5–9}. Thus, answering these fundamental questions is crucial for advancing applications based on plasmonic–2D hybridized systems.

Here we leverage a carefully optimized photonic heterostructure that enables the discovery and observation of a new family of neutral and charged dark excitons (that is, dark trions), and carefully study their features. Our heterostructure is formed by a WSe₂ monolayer coupled to optimized plasmonic cavities and encapsulated in tailored metal–insulator–semiconductor layers, which preserve the excitonic nature of monolayer and avoid unintentional doping. The observation of these spin-forbidden dark states in the absence of an external magnetic field is made possible by a remarkable enhancement factor of 3×10^5 . These dark exciton states feature ultranarrow linewidths of less than 0.4 meV (reaching the resolution limit) and a long lifetime of ~ 430 ps. To determine their features, we also studied their response to magnetic and electric field biases. We unequivocally reveal the spin-forbidden nature of these exciton states by applying an external magnetic field in two configurations, both perpendicular and parallel to the monolayer. These features enable us to draw the first solid conclusion about the observation of plasmonic cavity-enhanced spin-forbidden dark excitons, without unwanted doping effects. In addition, by varying the Fermi level in the WSe₂ monolayer via electric doping, we demonstrate the selective enhancement of dark trions and dark excitons. We also demonstrate how the emission intensity can be strongly modulated through electric doping in our heterostructure. Our findings broadly open new opportunities for hybrid nanophotonic devices that combine both active and passive components. Such hybrid devices are compact and compatible with a variety of platforms, including flexible and wavelength-multiplexed optoelectronics.

Results

Plasmonic heterostructure design and characterization

First, we describe the hybrid photonic platform investigated in this work. An array of site-controlled plasmonic nanocavities was fabricated with a standard ‘top-down’ approach, using electron-beam lithography and electron-beam metal evaporation (Methods). The lateral dimensions of the nanocubes range from $70 \times 70 \text{ nm}^2$ to $200 \times 200 \text{ nm}^2$, with a height of 100 nm. This design ensures that the excitons in the monolayer can consistently achieve optimal resonance with specific nanocubes (Supplementary Fig. 2). A hexagonal boron nitride (hBN)-encapsulated WSe₂ monolayer was placed between the bottom Au film and Au nanocubes (Fig. 1a), forming an extremely thin gap of <15 nm. We present the results from two hybrid structures with different hBN thicknesses. Our use of hBN encapsulation layers is critical to preserve the narrow linewidths of dark excitons and to optimize their coupling to the nanocavities without causing plasmonic doping. Figure 1b shows the optical image of sample number 1, whereas Fig. 1c presents the spatial mapping of the low-temperature (3.5 K) photonic emission from the sample on excitation with a 2.33 eV continuous-wave laser, as measured using an avalanche photodiode. For each spatial point in Fig. 1c, our measurements integrate the photoluminescence (PL) intensity for emission energies below 1.879 eV (dictated by the long-pass filter), showing a clear enhancement in the integrated PL occurring at the position of the nanocubes, with a maximum enhancement that the PL intensity is dominated by defect-bound states introduced during the fabrication process by comparing the PL spectra taken at both room and low temperatures from bare TMD flakes that were overexposed to the electron beam. These similar PL spectra confirm that there is no substantial defect introduced in the fabrication process (Supplementary Fig. 3).

We quantify the near-field of the plasmonic nanocavities that couple to the active TMD layer using numerical simulations (Fig. 1d). We focus on the $90 \times 90 \text{ nm}^2$ nanocubes in both simulations and experiments for the rest of the Article. The vertical field component $|E_z|$ of the dominant eigenmode for the selected geometrical parameters are shown in Fig. 1d. The in-plane field components for the same eigenmode are shown in Supplementary Fig. 1, using the same colour scale. These calculations demonstrate that within the nanogap in which the WSe₂ monolayer is placed, the strongly enhanced electric field is vertical, supporting selective coupling to excitons with out-of-plane dipole moments.

The plasmonic nanocavities enable the observation of a new family of exciton states with out-of-plane dipoles (Fig. 1a). In Fig. 2b, we identify a group of nine resonances with energies between 1.686 eV and 1.690 eV for an excitation power of 0.5 μW and a temperature of 1.6 K. By contrast, only a single dark exciton peak is detected when the nanocube is absent (Supplementary Fig. 4). These newly observed resonances are attributed to cavity-activated dark exciton states (CDs), denoted as CD₁–CD₉, whose spin-forbidden nature will be demonstrated in the following through the application of a magnetic bias. The emergence of these states results from a combination of features enabled by our heterostructure: suppressed plasmonic doping, ultrastrong out-of-plane electromagnetic field enhancement, cryogenic conditions and high-quality samples. In particular, the CDs feature ultranarrow linewidths smaller than 0.4 meV, the limit of spectral resolution, significantly narrower than previously reported spin-forbidden dark exciton states (~ 0.9 meV)¹⁸. We stress that this linewidth is also one of the narrowest ever reported for delocalized exciton states in a monolayer TMD^{20,21}, even though it may have already been broadened by the Purcell enhancement of the nanocavity. We also performed second-order correlation (g^2) measurements to rule out defect-bound single-photon emissions (Supplementary Fig. 5), often reported in WSe₂ (refs. 22,23). Therefore, the narrow linewidths are probably due to the intrinsic long lifetime of the exciton states ($\sim 430 \pm 30$ ps; Supplementary Fig. 6)

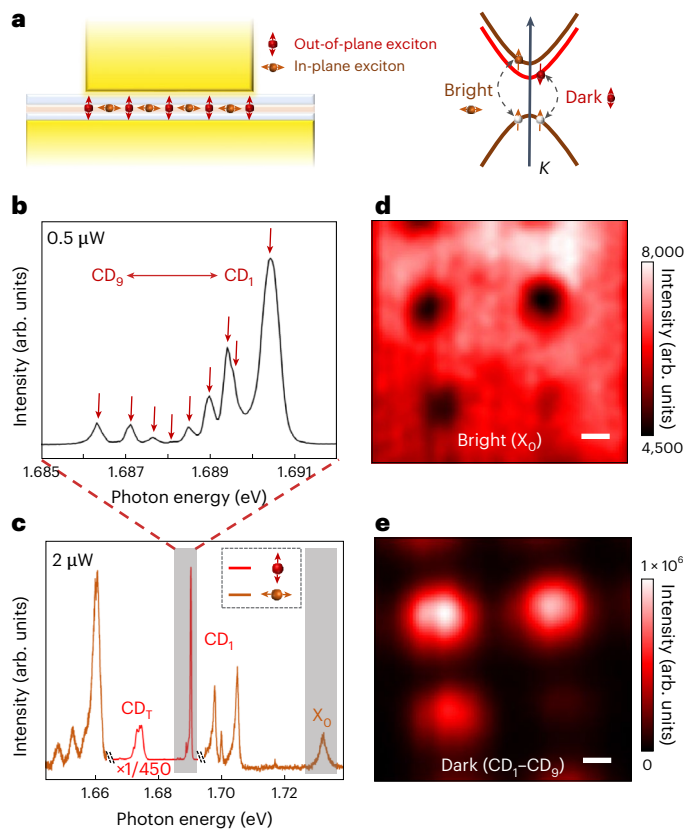


Fig. 2 | Plasmonic cavity unveiling new dark exciton resonances via selective field enhancement. **a**, Schematic of the cross-section of our hybrid photonic structures. The excitons with dipoles in different directions are situated inside the cavity (left). The dark exciton states exhibit both an out-of-plane dipole and the spin-forbidden transition (right). **b**, Fine structure of cavity-brightened dark exciton states with an excitation laser of 0.5 μW . Nine dark exciton states with narrow linewidths are clearly observed in PL. **c**, PL spectrum under an excitation laser of 2 μW . Excitons with two different dipole orientations are plotted using different coloured lines. Two resonances with out-of-plane dipoles are cavity-brightened dark exciton (CD_1) and cavity-brightened dark trion (CD_T). CD_1 has a linewidth of 0.38 meV. The out-of-plane exciton (CD_1) emissions have been attenuated by 450 times. **d, e**, Spatial PL mapping of bright excitons X_0 and dark excitons (CD_1 – CD_9). The intensity of each point in **d** or **e** is the integrated intensity over the spectral range indicated by the grey stripes in **c**. The intensity of the bright exciton is slightly reduced but that of dark excitons is dramatically enhanced via coupling to the plasmonic cavity. Scale bar, 200 nm.

and the high quality of our sample, combined with the extreme field confinement in the nanocavity.

To further investigate the enhancement selectivity of our hybrid nanophotonic platform, we measured the full PL spectrum of a single nanocavity coupled to the WSe_2 monolayer at an excitation power of 2 μW (Fig. 2c). We assigned the emission peaks to different exciton states (Supplementary Fig. 7) via their emission energy and validated these assignments by measuring the Zeeman splitting after applying a magnetic bias, and by studying the electric gating response, as presented later. Two types of out-of-plane dipole exciton were observed and drastically boosted by the nanocavity—dark excitons (CD_1 – CD_9) and a dark trion (CD_T). CD_1 showcases the most-prominent emission compared with the other dark excitons, due to its unique power-dependent enhancement (Supplementary Fig. 8). By contrast, excitons with in-plane dipole moments, including the bright exciton (X_0), retain their intrinsic characteristics of WSe_2 monolayers in the absence of nanocavity coupling (Fig. 2c and Supplementary Fig. 9). However, their emission was much weaker than the out-of-plane dipoles coupled to the nanocavity, due to the selective enhancement of plasmonic cavity.

By including hBN spacer layers, we effectively prevent plasmonic doping (Supplementary Fig. 10). Our finding suggests that the previously reported plasmonic-cavity-enhanced peak in a monolayer TMD^{5–9} should be attributed to charge-transfer-induced trions rather than cavity-enhanced dark excitons. To further demonstrate the on-site selective enhancement of different exciton states, we performed spatially resolved PL mapping. The spatial mapping for bright and dark excitons are shown in Fig. 2d,e, respectively. Although dark excitons are strongly boosted by the nanocavity, the emission from the bright exciton is suppressed. In addition to analysing the emission intensity of dark excitons, we also conducted a fitting of their emission energy (Supplementary Fig. 11). Interestingly, our analysis demonstrates that our nanocavities do not affect the resonance frequency.

Using the intensity of the bright exciton (X_0) as a reference, we evaluated the enhancement factor of the dark exciton (CD_1) according to the equation $\text{EF} = I_{\text{dark}} S_{\text{laser}} / I_{\text{bright}} S_{\text{nanocube}}$, where I_{dark} and I_{bright} are the fitted intensities of dark and bright excitons, respectively; S_{laser} is the diffraction-limited excitation laser spot size, around (953 nm)²; S_{nanocube} is the area under an individual nanocube, that is, the square of the nanocube edge length (90 nm). Sample number 1 has a total hBN thickness of 8 nm, which is thinner than the one of sample number 2 (15 nm), resulting in a stronger enhancement in CD emission. Specifically, the emission from CD_1 is 1,400 and 2,700 times stronger than the emission from X_0 in sample number 2 (Supplementary Fig. 12) and sample number 1, respectively. The enhancement factors of dark excitons of the two samples are estimated to be approximately 1.5×10^5 and 3×10^5 . To our knowledge, the enhancement demonstrated here represents a very high plasmonic enhancement in PL among various light-emitting materials, including quantum dots, 2D materials and fluorophores^{24–26}, owing to the specific layout of our hybrid nanophotonic platform, including the hBN encapsulation.

Magneto-optical response

To confirm the assignment of the newly discovered dark excitons to spin-forbidden dark transitions, we applied an external magnetic field (B_T) perpendicular to the 2D plane, corresponding to the Faraday geometry (Fig. 3a). As reported in earlier works, the short-range exchange interactions between the electron and hole in a WSe_2 monolayer lifts the valley degeneracy of the dark excitons, resulting in two eigenstates with different energies at $B_T = 0$ T (refs. 19,27), as illustrated in Fig. 3b. A false-colour map of our CD emission versus B_T is presented in Fig. 3c. Supplementary Fig. 13 displays the Zeeman splitting spectrum of these states at 4.5 T. We observe that each of the states (CD_1 – CD_9) splits into two peaks with an energy splitting $\delta = 0.66$ meV and a nonlinear dependence of the Zeeman splitting within a small-magnetic-field range ($-1 \text{ T} < B_T < 1 \text{ T}$). The higher-energy state of each Zeeman doublet is observable at a low magnetic field. Conversely, the lower-energy state is optically inactive, but it becomes visible when the magnetic field exceeds 1 T. Importantly, the Zeeman shift of these states is also identical.

We summarize the emission energy of the CD_1 doublet versus B_T in Fig. 3d as an example. The energy of the two states in each Zeeman doublet can be described as $E_{\pm} = E_0 + 0.5\sqrt{\delta^2 + (g\mu_B B_T)^2}$, where E_0 is the energy of the corresponding transition at zero magnetic field, g denotes the g -factor of the considered exciton complex and μ_B is the Bohr magneton. The measured Zeeman splitting can be used to verify the contribution of spin, valley and orbital magnetic moments in the TMD monolayer. The unique nonlinear dependence of Zeeman shift with $\delta = 0.66$ meV in the small-magnetic-field range is exclusive to spin-forbidden dark excitons²⁷, distinguishing them from other types of excitonic state, including both localized²⁸ and delocalized exciton states^{29,30}. Meanwhile, all exciton resonances CD_1 – CD_9 exhibit the same g -factor of 9.3 ± 0.1 , consistent with reported spin-forbidden dark excitons^{27,31}. Therefore, our observations strongly support our claim that the newly observed family of dark excitons CD_1 – CD_9 are spin-forbidden dark exciton states.

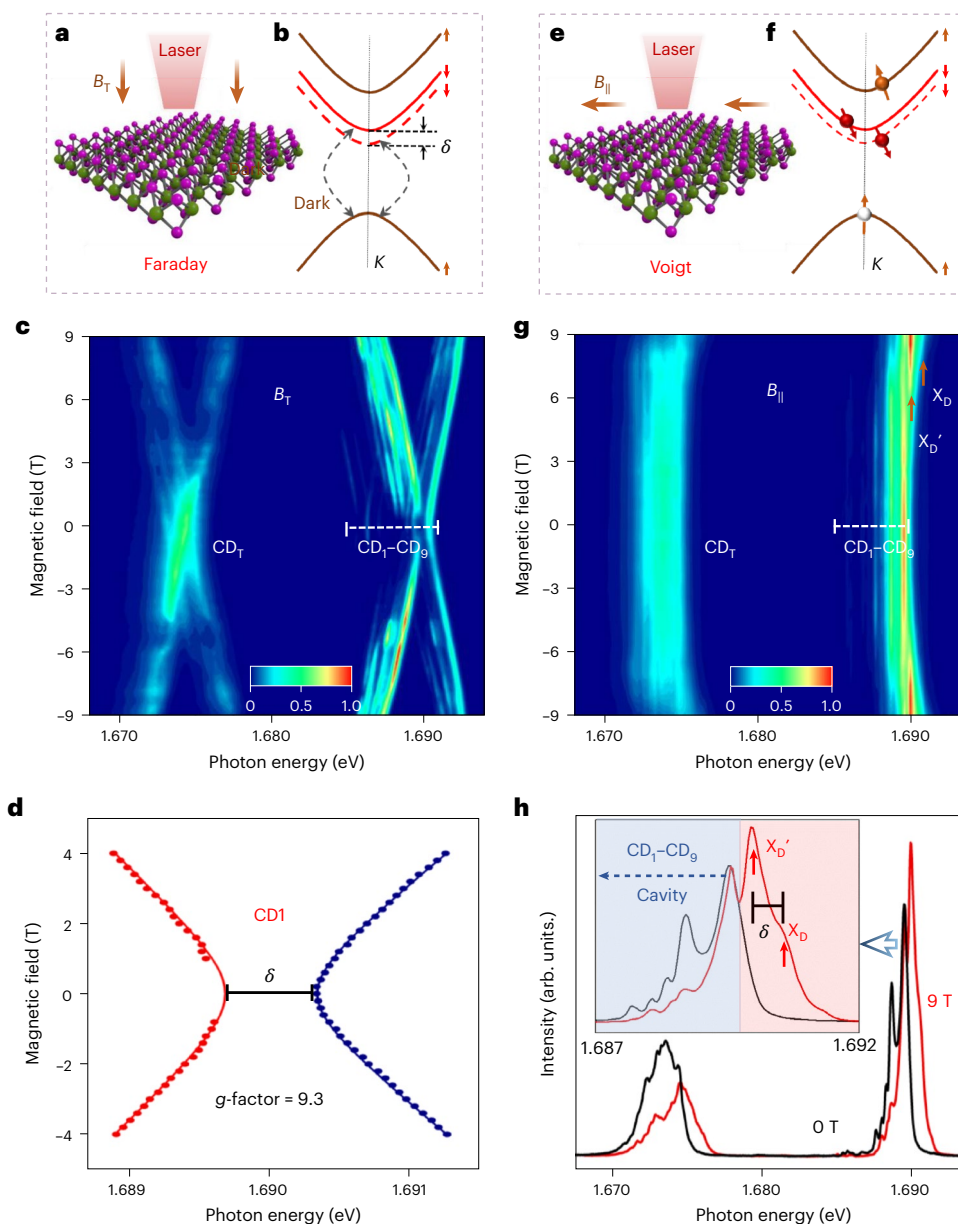


Fig. 3 | Properties of dark excitons in the presence of an external magnetic field. **a**, Schematic of the out-of-plane magneto-PL measurement in the Faraday configuration, that is, the B field perpendicular to the 2D plane. **b**, Exchange splitting of dark excitons due to the short-range exchange interaction. **c**, False-colour map of the PL spectra as a function of B_{\perp} . **d**, Energy shift of CD_1 as a function of B_{\perp} yielding its g -factor. **e**, Schematic of the in-plane magneto-PL

measurement in the Voigt configuration. **f**, Tilted spin polarization of electrons in the conduction band due to the in-plane magnetic field. **g**, False-colour map of the PL response as a function of the in-plane magnetic field. **h**, PL spectra measured with in-plane magnetic fields of 0 T and 9 T. The inset shows the zoomed-in spectrum of dark exciton states.

To be more precise, these states are better described as grey states as they are observable in the absence of an external magnetic field, for a sufficiently strong plasmonic enhancement factor^{27,32}.

An in-plane magnetic field (B_{\parallel}) can mix the spin components of the exciton states, which has been proved to be an effective way to brighten dark excitons^{19,33} (Fig. 3e,f). The 2D false-colour map of the PL spectra as a function of B_{\parallel} is presented in Fig. 3g. The spectra with B_{\parallel} of 0 T and 9 T are displayed in Fig. 3h. In particular, as B_{\parallel} increases, the CD dark excitons weaken, whereas two new exciton states at higher energy emerge with $\delta = 0.66$ meV. The enhanced emission observed in the presence of B_{\parallel} , with the same δ , suggests that they are conventional spin-forbidden dark exciton states whose valley degeneracy is lifted by the short-range exchange interaction. We label these resonances as X_D and X_D' . X_D is the spin-forbidden dark exciton following previous

experiments on WSe_2 monolayers without cavity enhancement^{27,31}. By contrast, X_D' is both spin forbidden and electric dipole forbidden, which is only observable in the presence of an external magnetic field⁸. The distinct response to B_{\parallel} indicates that the CDs are distinct from conventional dark excitons, despite sharing the feature of being spin forbidden with an out-of-plane dipole. As spin mixing induced by B_{\parallel} can perturb the excitonic wavefunction, it reduces the purity of the out-of-plane dipole moment of the spin-forbidden dark excitons. This reduction breaks the strict selection rule and significantly enhances the PL of conventional dark excitons. However, for CDs, the modified out-of-plane dipole weakens the coupling between the CDs and the plasmonic mode, leading to a suppression of their emission intensity. Meanwhile, the absence of X_D at $B_{\parallel} = 0$ T implies that the plasmonic nanocavity has a stronger affinity to our CDs than to conventional dark exciton states.

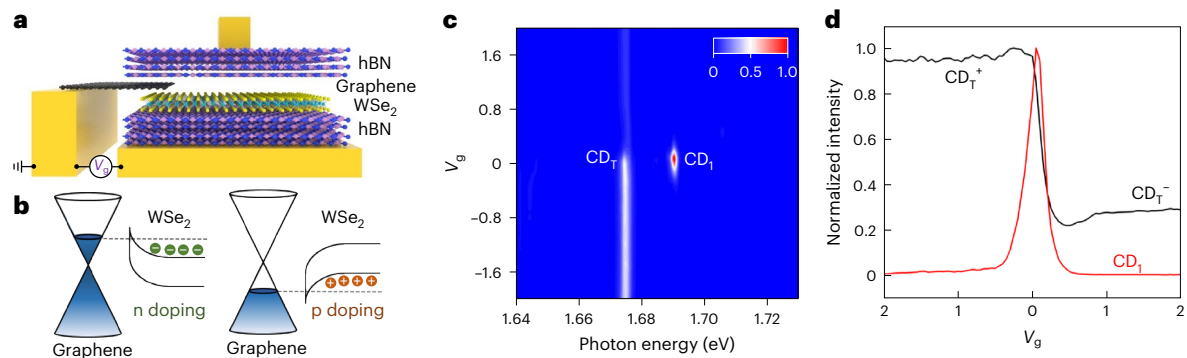


Fig. 4 | Selective activation of new dark excitons via electric doping. **a**, Schematic of the electric doping device. The bottom Au film and a few-layer-thick graphene layer are used as gates. **b**, Schematic of electrical doping. When a voltage is applied, electrons or holes can be injected into the WSe₂ monolayer via graphene. **c**, Normalized PL intensity as a function of back

gate voltage and photon energy. **d**, Normalized emission intensities of CD₁ and CD₁ as a function of V_g. The intensity of CD₁ is switched around the voltage of charge neutrality by a change of 0.3 V due to the transition between negative dark trion (CD₁⁻) and positive dark trion (CD₁⁺).

Electrostatic doping

The intensity of dark excitons and trions can be selectively controlled through electric doping. We used the bottom Au film and a few-layer-thick graphene layer as gates to demonstrate electric control (Fig. 4a and Supplementary Fig. 12). By applying a gate voltage (V_g), we electrostatically dope the monolayer WSe₂, modifying its Fermi level (Fig. 4b). Figure 4c shows the PL intensity from sample number 2 as a function of V_g and photon energy. The intensity of CD₁ is sensitive to the carrier density as the oscillator strength is quickly transferred to the charged trion states outside a narrow range of doping density, and thus, its intensity drops quickly with the applied voltage. This underscores the importance of controlling the plasmon-induced doping effect when investigating plasmonic–2D hybrid systems. By contrast, the intensity of CD₁ appears binary, that is, it switches between two discrete values due to the formation of either a negative or a positive trion^{34,35}. The measured emission intensities are shown in Fig. 4d as a function of V_g. Interestingly, the intensity of CD₁ can be effectively switched by a small voltage of 0.3 V. The PL intensity associated with CD₁⁺ is three times stronger than that with CD₁. This type of binary switching makes the electric control of dark exciton emission highly promising for signal transduction in optoelectronic devices.

Discussion

In conclusion, we conclusively unveiled a family of dark excitons in WSe₂ monolayers, enabled by an exceptionally large enhancement factor from coupling to plasmonic nanocavities. By applying an external magnetic field parallel or perpendicular to the monolayer, we confirmed their spin-forbidden dark exciton nature, with dipole moments perpendicular to the 2D plane. These results enable us to draw the first solid conclusion about the observation of plasmonic cavity-enhanced spin-forbidden dark excitons. Meanwhile, given the extensive progress in integrating 2D materials with engineered photonic systems, the incorporation of these dark excitons into emerging platforms—including on-chip integrated photonics—offers new opportunities for on-site enhancement and tunability through magneto-optical effects and electrostatic doping. Our top-down fabrication approach provides a scalable and cost-effective route towards site-controlled nanoscopic light sources. In addition to the prospects outlined in this paper for nanophotonic and optoelectronic devices, we also resolve the long-standing debate about the role of plasmonic interactions in exciton physics, and demonstrate that it is possible to preserve their nature and drastically enhance their optical emission properties. These findings pave the way for future experiments incorporating semiconductor moiré systems, where periodically modulated

potential landscapes and the chiral selection rules of valley excitons in a well-defined array may open exciting prospects for the realization of highly tunable quantum metasurfaces.

Online content

Any methods, additional references, Nature Portfolio reporting summaries, source data, extended data, supplementary information, acknowledgements, peer review information; details of author contributions and competing interests; and statements of data and code availability are available at <https://doi.org/10.1038/s41566-025-01788-w>.

References

- Mak, K. F., Lee, C., Hone, J., Shan, J. & Heinz, T. F. Atomically thin MoS₂: a new direct-gap semiconductor. *Phys. Rev. Lett.* **105**, 136805 (2010).
- Malic, E. et al. Dark excitons in transition metal dichalcogenides. *Phys. Rev. Mater.* **2**, 014002 (2018).
- Mai, C. et al. Many-body effects in valleytronics: direct measurement of valley lifetimes in single-layer MoS₂. *Nano Lett.* **14**, 202–206 (2014).
- Chand, S. B. et al. Interaction-driven transport of dark excitons in 2D semiconductors with phonon-mediated optical readout. *Nat. Commun.* **14**, 3712 (2023).
- Park, K. D., Jiang, T., Clark, G., Xu, X. & Raschke, M. B. Radiative control of dark excitons at room temperature by nano-optical antenna-tip Purcell effect. *Nat. Nanotechnol.* **13**, 59–64 (2018).
- Lo, T. W. et al. Plasmonic nanocavity induced coupling and boost of dark excitons in monolayer WSe₂ at room temperature. *Nano Lett.* **22**, 1915–1921 (2022).
- Zhou, J. et al. Near-field coupling with a nanoimprinted probe for dark exciton nanoimaging in monolayer WSe₂. *Nano Lett.* **23**, 4901–4907 (2023).
- Hasz, K., Hu, Z., Park, K. D. & Raschke, M. B. Tip-enhanced dark exciton nanoimaging and local strain control in monolayer WSe₂. *Nano Lett.* **23**, 198–204 (2023).
- Rahaman, M. et al. Observation of room-temperature dark exciton emission in nanopatch-decorated monolayer WSe₂ on metal substrate. *Adv. Opt. Mater.* **9**, 2101801 (2021).
- Wen, X. et al. Pathways of exciton triggered hot-carrier injection at plasmonic metal–transition metal dichalcogenide interface. *Adv. Opt. Mater.* **10**, 2100070 (2022).
- Shan, H. et al. Direct observation of ultrafast plasmonic hot electron transfer in the strong coupling regime. *Light: Sci. Appl.* **8**, 9 (2019).

12. Deng, M. et al. Light-controlled near-field energy transfer in plasmonic metasurface coupled MoS₂ monolayer. *Small* **16**, 2003539 (2020).
13. Brongersma, M. L. Plasmon-induced hot carrier science and technology. *Nat. Nanotechnol.* **10**, 25–34 (2015).
14. Kang, Y. et al. Plasmonic hot electron induced structural phase transition in a MoS₂ monolayer. *Adv. Mater.* **26**, 6467–6471 (2014).
15. Liu, H. et al. Spontaneous chemical functionalization via coordination of Au single atoms on monolayer MoS₂. *Sci. Adv.* **6**, eabc9308 (2020).
16. He, Z. et al. Quantum plasmonic control of trions in a picocavity with monolayer WS₂. *Sci. Adv.* **5**, eaau8763 (2019).
17. Shi, J. et al. Enhanced trion emission and carrier dynamics in monolayer WS₂ coupled with plasmonic nanocavity. *Adv. Opt. Mater.* **8**, 2001147 (2020).
18. Li, Z. et al. Emerging photoluminescence from the dark-exciton phonon replica in monolayer WSe₂. *Nat. Commun.* **10**, 2469 (2019).
19. Robert, C. et al. Measurement of the spin-forbidden dark excitons in MoS₂ and MoSe₂ monolayers. *Nat. Commun.* **11**, 4037 (2020).
20. Barbone, M. et al. Charge-tuneable biexciton complexes in monolayer WSe₂. *Nat. Commun.* **9**, 3721 (2018).
21. He, M. et al. Valley phonons and exciton complexes in a monolayer semiconductor. *Nat. Commun.* **11**, 618 (2020).
22. Koperski, M. et al. Single photon emitters in exfoliated WSe₂ structures. *Nat. Nanotechnol.* **10**, 503–506 (2015).
23. Parto, K., Azzam, S. I., Banerjee, K. & Moody, G. Defect and strain engineering of monolayer WSe₂ enables site-controlled single-photon emission up to 150 K. *Nat. Commun.* **12**, 3585 (2021).
24. Akselrod, G. M. et al. Probing the mechanisms of large Purcell enhancement in plasmonic nanoantennas. *Nat. Photon.* **8**, 835–840 (2014).
25. Hoang, T. B. et al. Ultrafast spontaneous emission source using plasmonic nanoantennas. *Nat. Commun.* **6**, 7788 (2015).
26. Huang, J., Akselrod, G. M., Ming, T., Kong, J. & Mikkelsen, M. H. Tailored emission spectrum of 2D semiconductors using plasmonic nanocavities. *ACS Photonics* **5**, 552–558 (2018).
27. Robert, C. et al. Fine structure and lifetime of dark excitons in transition metal dichalcogenide monolayers. *Phys. Rev. B* **96**, 155423 (2017).
28. Dang, J. et al. Identifying defect-related quantum emitters in monolayer WSe₂. *npj 2D Mater. Appl.* **4**, 2 (2020).
29. Aivazian, G. et al. Magnetic control of valley pseudospin in monolayer WSe₂. *Nat. Phys.* **11**, 148–152 (2015).
30. Srivastava, A. et al. Valley Zeeman effect in elementary optical excitations of monolayer WSe₂. *Nat. Phys.* **11**, 141–147 (2015).
31. Li, Z. et al. Momentum-dark intervalley exciton in monolayer tungsten diselenide brightened via chiral phonon. *ACS Nano* **13**, 14107–14113 (2019).
32. Molas, M. R. et al. Probing and manipulating valley coherence of dark excitons in monolayer WSe₂. *Phys. Rev. Lett.* **123**, 096803 (2019).
33. Zhang, X. X. et al. Magnetic brightening and control of dark excitons in monolayer WSe₂. *Nat. Nanotechnol.* **12**, 883–888 (2017).
34. Liu, E. et al. Gate tunable dark trions in monolayer WSe₂. *Phys. Rev. Lett.* **123**, 027401 (2019).
35. Li, Z. et al. Direct observation of gate-tunable dark trions in monolayer WSe₂. *Nano Lett.* **19**, 6886–6893 (2019).

Publisher's note Springer Nature remains neutral with regard to jurisdictional claims in published maps and institutional affiliations.

Springer Nature or its licensor (e.g. a society or other partner) holds exclusive rights to this article under a publishing agreement with the author(s) or other rightsholder(s); author self-archiving of the accepted manuscript version of this article is solely governed by the terms of such publishing agreement and applicable law.

© The Author(s), under exclusive licence to Springer Nature Limited 2025

¹Photonics Initiative, Advanced Science Research Center, City University of New York, New York, NY, USA. ²Department of Physics, Complex Quantum Systems, and Texas Materials Institutes, The University of Texas at Austin, Austin, TX, USA. ³Research Center for Electronic and Optical Materials, National Institute for Materials Science, Tsukuba, Japan. ⁴Research Center for Materials Nanoarchitectonics, National Institute for Materials Science, Tsukuba, Japan. ⁵Physics Program, The Graduate Center, The City University of New York, New York, NY, USA. ⁶Present address: School of Physical Science and Engineering, Tongji University, Shanghai, China. ✉e-mail: elaineli@physics.utexas.edu; aalu@gc.cuny.edu

Methods

Plasmonic heterostructure fabrication

The plasmonic cavity was fabricated with a ‘top-bottom’ approach. We start from substrates composed of a 285-nm-thick layer of silicon dioxide on top of bulk silicon. A layer of 950 poly(methyl methacrylate) (PMMA) A4 was spin coated on the substrate at a speed of 3,000 rpm for 60 s to achieve a thickness of 200 nm, followed by baking at 180 °C for 60 s. The patterns of the Au mirror (back gate) and contact gate were written with an Elionix ELS-G50 electron-beam lithography system and developed in methyl isobutyl ketone–isopropanol at a ratio of 1:3 for 20 s. Afterwards, 1 min of O₂ plasma (100 W) was used to remove the remaining PMMA on the pattern. A 5-nm Cr adhesion layer and a 95-nm Au layer were deposited by slow-rate electron-beam evaporation under a high vacuum and then lifted off by acetone. The gap between the Au mirror and contact gate is kept to 2 μm to avoid strain production during the transfer process of the 2D heterostructure. The hBN-encapsulated monolayer WSe₂ was transferred onto the Au film immediately. Then, a 200-nm-thick layer of 495 PMMA A4 and 250-nm-thick layer of 950 PMMA A4 were spun on the substrate. To reduce the charging of the non-conductive hBN, a 10-nm Au layer was deposited on top of the resist. The pattern of Au nanocubes was written using an Elionix ELS-G100 electron-beam lithography system. After removing the anti-charging layer, the resist was developed in methyl isobutyl ketone–isopropanol at a ratio of 1:3 for 60 s. The 100-nm Au layer was then deposited on the sample to form the nanocubes. Finally, a lift-off step was performed in acetone for 2 h to obtain the Au nanocubes.

Fabrication of 2D hBN-encapsulated monolayer WSe₂ device

We fabricated the hBN-encapsulated monolayer WSe₂ device by the well-known dry transfer technique^{36,37}. The monolayer WSe₂ (HQ Graphene) and few-layer hBN are first exfoliated onto a 285-nm SiO₂/Si substrate. The thicknesses of those layers are measured by atomic force microscopy. Afterwards, the polypropylene carbonate stamp sequentially picks up the few-layer hBN, few-layer graphene, monolayer WSe₂ and another few-layer hBN. The complete stack is released onto the Au film at 120 °C. The few-layer graphene extends out of the bottom hBN layer to touch with the contact gate. During the dropping process, bubbles formed between the individual van der Waals layers are squeezed out of the stack at a temperature of around 90 °C. The sample is then rinsed in acetone to remove the melted polypropylene carbonate.

PL spectroscopy

PL measurements were performed at 1.6 K using a closed-cycle cryogen-free cryostat (attoDRY2100). Magnetic fields within the range of 0–9 T were applied in the Voigt configuration (magnetic field parallel to the layer plane) or Faraday configuration (magnetic field perpendicular to the layer plane). The numerical apertures of the objective lens were 0.81 and 0.63 for the Faraday and Voigt configurations, respectively. V_g was applied to the back gate through a Keithley 2400 source meter and the graphene layer was grounded. The intensity mapping, spectrum mapping, g^2 measurement and lifetime measurement were performed at 6 K in a custom-built confocal microscope setup coupled to a closed-cycle cryostat (Montana). A continuous-wave green laser (2.33 eV) with a power of 1 μW was used for intensity mapping, spectrum mapping and g^2 measurement. A pulsed laser excitation centred at 1.959 eV (NKT, SuperK Fianium) and with an excitation power of 2 μW was used for lifetime measurement. The mappings were taken with a galvanometer mirror scanner in the 4f configuration. The diffraction-limited spatial resolution is ~350 nm. An objective with a numerical aperture of 0.9 was used for high-efficiency collection. The

g^2 measurement and lifetime measurement were spectrally filtered by a custom-built monochromator with a resolution of 1 nm. The lifetime measurement was collected using the time-correlated single-photon counting technique with a single-photon detector (PicoQuant) employing time-resolved single-photon counting (PicoQuant, PicoHarp 300). The lifetimes of the different excitonic complexes were fitted by a single exponential function $I = Ae^{-t/\tau}$. Second-order correlation functions g^2 are measured in Hanbury–Brown and Twiss with free-space-coupled avalanche photodiodes.

Data availability

The main data supporting the findings of this study are available within the Article and its Supplementary Information. Additional data are available from the corresponding authors on request.

References

36. Wang, L. One-dimensional electrical contact to a two-dimensional material. *Science* **342**, 614–617 (2013).
37. Purdie, D. G. et al. Cleaning interfaces in layered materials heterostructures. *Nat. Commun.* **9**, 5387 (2018).

Acknowledgements

This work was primarily supported by the Air Force Office of Scientific Research, the Office of Naval Research, the National Science Foundation and the Simons Foundation. Z.L. and X.L. were partially funded by the National Science Foundation via grant numbers NSF ECCS-2130552 and MRSEC DMR-2308817. X.L. gratefully acknowledges support from Welch Foundation chair F-0014. G.G. acknowledges partial support from the National Science Foundation (DMR-2044281) and from the Graduate Center of CUNY. K.W. and T.T. acknowledge support from the JSPS KAKENHI (grant numbers 21H05233 and 23H02052) and World Premier International Research Center Initiative (WPI), MEXT, Japan. We gratefully acknowledge helpful discussions with E. Malic from Philipps-Universität Marburg and C. H. Lui from the University of California, Riverside.

Author contributions

J.Q., A.A. and X.L. conceived the idea. J.Q. led the optical experiments, with assistance from M.C., S.C., X.J., Z.L. and E.M. M.C. led the numerical simulations. J.Q. prepared the sample with contributions from M.C. and X.J. T.T. and K.W. provided the hBN sample. J.Q., A.A. and X.L. wrote the manuscript. A.A., X.L. and G.G. supervised the project. All authors discussed the results.

Competing interests

The authors declare no competing interests.

Additional information

Supplementary information The online version contains supplementary material available at <https://doi.org/10.1038/s41566-025-01788-w>.

Correspondence and requests for materials should be addressed to Xiaoqin Li or Andrea Alù.

Peer review information *Nature Photonics* thanks the anonymous reviewers for their contribution to the peer review of this work.

Reprints and permissions information is available at www.nature.com/reprints.